

EVLA Memo 85

Testing the EVLA L-Band Feed

Rick Perley, Bob Hayward, and Dan Mertely
NRAO

November 16, 2004

Abstract

Total-power tests of the new EVLA L-band feed at 1425 MHz show an efficiency of 43%, and a cold-sky system temperature of 27K, giving a System Equivalent Flux Density (SEFD) of 335 Jy, approximately the same as the current VLA L-band feed. The new feed, however, sees very much less ground spillover, resulting in a significant overall performance improvement for long-duration experiments which include significant low-elevation integration. The efficiency of the new feed increases with increasing frequency, reaching 54% at 1975 MHz. The location of the phase center varies as expected with frequency, but will not result in significant loss in gain when an optimum subreflector position is utilized. The antenna's beamwidth and inner sidelobe structures are as expected from performance simulations, and are nearly indistinguishable from those of the VLA antennas at 1425 MHz.

1 Introduction

A primary requirement for the EVLA is to provide eight high-performance wide-bandwidth feeds and receivers operating from the Cassegrain feed ring. For the lowest-frequency band (L-band), this requires a feed operating from 1.2 to 2.0 GHz. This feed must fit within the restricted space available on the VLA Cassegrain feed ring, a constraint which limited the maximum aperture to 62 inches, about 50% less than that considered optimum for illuminating the subreflector at this frequency. Despite this difficult constraint, a feed designed by S. Srikanth to provide good performance over the 800 MHz bandwidth was built and installed on the EVLA Test Antenna (antenna 13) for testing.

In this report, we report on the results of performance tests on this feed. The parameters measured were: the cold-sky system temperature, the illumination spillover, the antenna efficiency, the location of the phase center, and the antenna power pattern, including the nearby sidelobes. These parameters were determined at four frequencies: 1325, 1425, 1675, and 1975 MHz. For comparison purposes, similar tests at 1425 MHz only were made on two antennas equipped with the VLA's current L-band feed.

2 Measurement Methodology

The measurements we are reporting were taken during September, 2004, when IF system was at the AOC in Socorro for system integration. We thus used a simple total-power system at the output of the RF cooled receiver. Without an IF downconversion capability, the frequencies and bandwidths chosen were set by the filters that were available at the time of the observations: 1325/50, 1425/60, 1675/50 and 1975/60 MHz.

The test setup utilized was very straightforward, and is depicted in Fig 1. The output signal from either the R or L channel of the cooled receiver was amplified, passed through a limiting RF

filter, detected by a square-law detector, and the power recorded by a digital power meter. These data were recorded on a laptop for subsequent analysis. The FE's internal noise diode was used to assist in calibration. Because all data were reduced 'by hand', the switching of the noise diode had to be reduced to typically 0.1 Hz rate. The power meter smoothed the data stream internally, and dumped samples at a 1 Hz rate to the recording laptop.

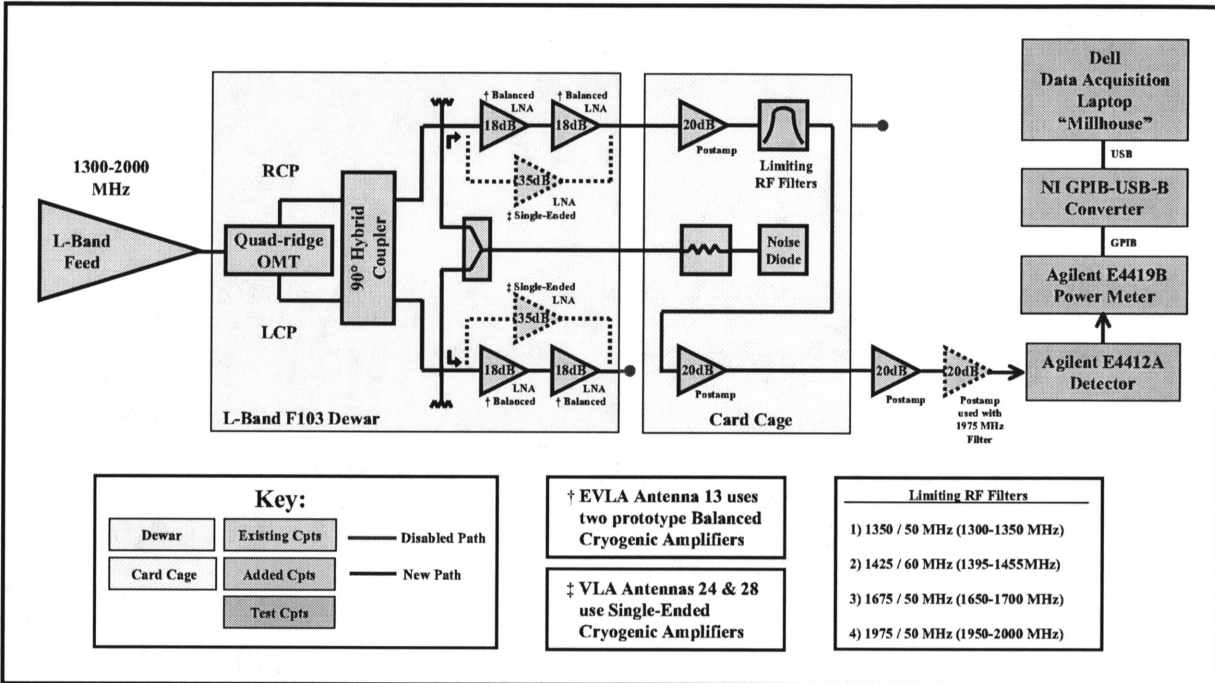


Figure 1: The measurement setup for determining the EVLA's L-Band antenna performance. The blue box contains the cryogenically cooled components. Note that the cooled amplifiers for the EVLA are a pair of balanced amplifiers, rather than a single high-gain stage used for the VLA antennas (shown by the dashed components). The yellow box contains the initial postamps – normally the two polarizations each pass through a single 20 dB amplifier. For our measurements, a higher output power was needed for stable detection with the power meter, so we chained the two postamps within the Card Cage, then added one or two more postamps to reach the desired -20dBm power level.

Considerable effort was put into stabilizing the power detector/recording system. It was found that instabilities in the detection system required power input levels of typically -30 dBm or higher. As the input noise power, $kT\Delta\nu$, is typically -110 dBm , at least 80 dB of gain was needed to ensure stable data. This required three to four amplifiers between the FE output and the power detector. A curious non-linearity was discovered when power levels of -10dBm was achieved – this problem, and our methodology for calibration of the data, are described in the next section.

The data were taken during September, 2004. The characteristics we measured, and the means of determining them, are briefly described below.

2.1 Focus Curve

A characteristic of the compact horn design selected for the L-band feed is a significant variation of the location of the effective phase center with frequency. For the EVLA L-band horn, the phase center drops by 246 cm between 1.0 and 2.0 GHz, and by 203 cm between the nominal design frequencies of 1.2 and 2.0 GHz. The expected corresponding range of motion for the subreflector is

reduced by the square of the magnification to about 3 cm between 1.2 and 2.0 GHz, and to about 2.5 cm between 1.4 and 2.0 GHz.

The subreflector's location for maximum forward gain, and the focus loss curve was determined at the four frequencies by moving the subreflector over its range of motion while observing the strong radio source Cygnus A.

2.2 Illumination Spillover and Scattering

The system temperature is expected to increase at low elevations due to scattering of ground radiation off the quadrupod legs, subreflector, and other structures into the feed. At very low elevations, direct spillover from the ground into the feed will be seen. Scattering of ground radiation into the horn is very strong with the existing L-band feed, which utilizes a microwave lens to reduce the size of the horn. The new feed design eliminates the lens, and we expect a much reduced variation of system temperature with elevation.

To measure the spillover, the antenna was driven manually from 90 degrees elevation to 8 degrees at an azimuth which ensured minimal contamination from galactic plane emission. This was done initially in 5 or 10 degree steps, but it was subsequently found to be considerably more efficient and convenient to drive the antenna continuously. Over-the-top measurements, to the antenna's maximum elevation of 125 degrees, were also performed to check the symmetry of the spillover.

2.3 Cold Sky System Temperature

The new feed system does not require a lens, and we thus expect a small improvement of a few Kelvin in system temperature due to the absence of this lossy device. A further improvement is expected from the replacement of the dielectric polarizer with a cooled hybrid polarizer.

This crucial sensitivity parameter was determined by high-elevation observations of the cold sky, taken during the tipping observations described above.

2.4 Antenna Efficiency

The new L-band horn is necessarily undersized due to the lack of space around the cassegrain feed ring. The efficiency of the feed, especially at the lower end of the band, is thus expected to be poorer than the existing feed at these frequencies – a loss of sensitivity which we expect to be offset by an improved system temperature due to the removal of the lens, and, for continuum observations, the greatly increased bandwidth.

The efficiency of the feed was measured through observations of a source of known flux density. The increment in system power is a direct measure of the efficiency.

2.5 Antenna Beamwidth and Sidelobes

The width and sidelobe levels of the primary beam are sensitive functions of the illumination of the primary reflector. Measurement of these requires scanning the antenna response through a strong source. Radial scans through Cygnus A, extending about 2.5 degrees on each side of the beam maximum, were made to measure the size and shape of the main response lobe, and the inner two sidelobes. Cuts at either four or eight different position angles were made of the EVLA Test Antenna at 1425 and 1975 MHz. For comparison, four cuts through a VLA antenna beam were made at 1425 MHz.

3 Data Calibration

The various observations were taken at four frequencies with varying amounts of gain and output power. If we presume there is no zero offset, and the measured output power is a linear function of the input power, we can write $P = GT$, where P is the power measured by the power meter (in mW), T is the input power expressed in temperature units (so $P_{in} = kT\Delta\nu$), and G is the system gain, with units mW/K¹. The constant G is determined by a ‘hot load’ measurement – covering the feed with a black-body absorber of known physical temperature T_{abs} , and noting the power detected P_h . The input power is the sum of the contributions from the absorber and the receiver itself, so $P_h = GT_h = G(T_{abs} + T_r)$, where T_r is the receiver temperature². The calibration coefficient needed to convert any other observation from mW to degrees Kelvin will be

$$K = G^{-1} = \frac{T_{abs} + T_r}{P_h}. \quad (1)$$

In practice, the receiver temperature is known from bench calibrations with an accuracy of a few Kelvin – an error which is negligible in comparison to the absorber temperature, typically 300K.

From this calibration, the noise diode’s temperature contribution can be determined as $\Delta T = K\Delta P$, where ΔP is the increment in the detected power due to the noise diode. A useful check on the validity of the procedure is to compare the value determined in this way to that from bench measurements.

The requirement for zero offset is easily assured, as the power meter has a zero-offset feature. The linearity assumption can be checked by comparing the increment in power due to the switched noise diode when observing the hot load to that when on cold sky. In fact, we noted that when the power input to the meter was at the higher levels (–10 dBm was the highest we used), there was a surprising non-linearity – the observed output power increment from the noise diode while observing on the hot load was up to 50% larger than that measured while on the cold sky! This very non-intuitive behavior (which is the opposite expected when an amplifier nears saturation) was repeatable, and considerable time and effort were expended to understanding its characteristics. These efforts demonstrated that the problem was not due to the noise diode’s power increment being a function of input power, but originates either in our using three or more post-amps after the FE in order to raise the signal level high enough for stable detection, or in the power detection system itself.

Our tests indicated that the non-linearity was stable and repeatable for any given amplifier setup, so a non-linear gain calibration should be possible. If we write the gain relation as

$$P = GT + HT^2 \quad (2)$$

we can determine the two system constants, G and H by utilizing two constraints:

1. The power detected with a hot load of known temperature:

$$P_h = G(T_{abs} + T_r) + H(T_{abs} + T_r)^2, \quad (3)$$

and

2. The power added by the switched noise source is the same when on hot and cold loads. This condition can be written

$$\frac{\Delta P_h}{G + 2HT_h} = \frac{\Delta P_c}{G + 2HT_c} \quad (4)$$

¹In this formulation, the gain G incorporates Boltzmann’s constant k and the system bandwidth $\Delta\nu$.

²Other sources of input power can be postulated: sky emission leaking through the absorber, or through cracks in the feed horn, or emission from the horn itself. Tests showed these to be negligible in comparison to the identified sources.

In these expressions,

- ΔP_h and ΔP_c are the measured output power increments due to the noise diode when on the hot load and cold sky respectively,
- $T_h = T_{abs} + T_r$ is the total hot load temperature,
- T_c is the total cold sky temperature, comprising a sum of the receiver temperature, atmospheric emission, the cosmic microwave background, galactic plane emission, and ground spillover contributions.

As the contributions to T_c are not accurately known, T_c must be expressed in terms of the measured cold power, P_c , and the system gain constants, G and H , through equation 2.

The gain constants, G and H , and the noise diode temperature, ΔT , can then be determined from the observed hot load power P_h , cold sky power P_c , the known hot load temperature T_h , and the observed switched power increments ΔP_c and ΔP_h . We find

$$G = \frac{2A}{BT_h} \left(\sqrt{1 + \frac{BP_h}{A}} - 1 \right) \quad (5)$$

$$H = \frac{P_h - GT_h}{T_h^2} \quad (6)$$

$$\Delta T = \frac{\Delta P_h}{G + 2HT_h}. \quad (7)$$

where

$$A = P_h - Y^2 P_c \quad (8)$$

$$B = Y^2 - 1 \quad (9)$$

and

$$Y = \frac{\Delta P_h}{\Delta P_c}. \quad (10)$$

With these, the antenna temperature of a given power determination can be expressed as

$$T = \frac{G}{2H} \left(\sqrt{1 + \frac{4HP}{G^2}} - 1 \right). \quad (11)$$

In practice, the non-linear analysis was required only for a few test runs on the VLA antennas, where extra amplification was required due to a low output power from the FE.

4 Results

4.1 Focus Location

Focus curves were measured at all four frequencies, with the results shown in Fig. 2. As expected, there is a small, ~ 2 cm shift in optimum subreflector position between 1325 and 1975 MHz. Notable is the lack of significant difference between 1675 and 1975 MHz. This is an expected result of the feed design. We were unable to make measures at a frequency lower than 1325 MHz, where the design predicts an increasing rate of phase center offset. However, we are fortunate that the focus curve broadens with lower frequency, so that even if the focal point accelerates its position upwards, there will be negligible effect on system efficiency from using a single subreflector position near -2.5 cm.

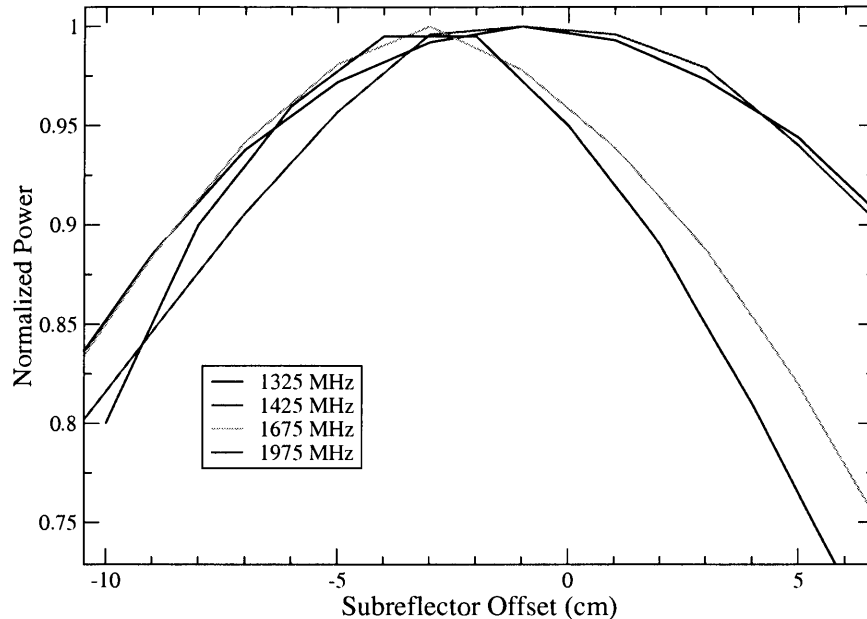


Figure 2: The normalized power as a function of subreflector position. A higher subreflector position is to the right in this plot. The optimum position drops by about 2cm between the lower pair of frequencies (1325 and 1425 MHz) and the higher frequencies. There is little change in optimum subreflector position between the upper pair of frequencies, as expected. At the optimum position of -2.5 cm, the loss of gain at any frequency is less than 1%. The subreflector offset at which the forward gain drops by 20% is 10.5, 9.5, 8, and 6.5 cm for 1325, 1425, 1675, and 1975 MHz, respectively, from each frequency’s optimum position.

4.2 Illumination Spillover

The VLA’s L-band feed combines an undersized horn illuminating a microwave lens located about five feet above the horn. This lens is composed of a central dielectric surrounded by a ring of short metal cylinders. The lens scatters ground radiation into the feed when observing at elevations less than ~ 60 degrees. An important design requirement for the new EVLA feed is to minimize this unwanted source of system temperature. Another contribution to the variation in system temperature with elevation is spillover of the illumination pattern beyond the antenna main reflector. This contribution is not expected to differ significantly between the VLA and EVLA designs.

To measure the contributions from scattering, spillover, and atmospheric emission, sky dips were made with the EVLA test antenna at all four frequencies, and with two VLA antennas at a single frequency of 1425 MHz. An example of one of the EVLA sky dips is shown in Fig. 3.

The system temperature, and the derived spillover, as a function of elevation for the four frequencies are shown in Fig. 4. The left panel shows the total system temperature, as a function of elevation, for the four test frequencies. The data at 1975 MHz were taken with a low-gain FE system, resulting in a high system temperature. Consequently, we have offset the data shown in the figure by 88K from their observed values – the data as shown correspond to what the new receiver should provide. The higher overall system temperature at 1675 MHz is likely due to a higher receiver noise temperature at that frequency³. The right panel shows the variation of spillover contribution with elevation. These values were derived by first subtracting the expected

³Table 1 shows that the lab determination of the receiver temperature at 1675 MHz to be only one degree higher than at 1425 MHz, while the sky dip observations indicate the difference to be five degrees. This discrepancy is not understood.

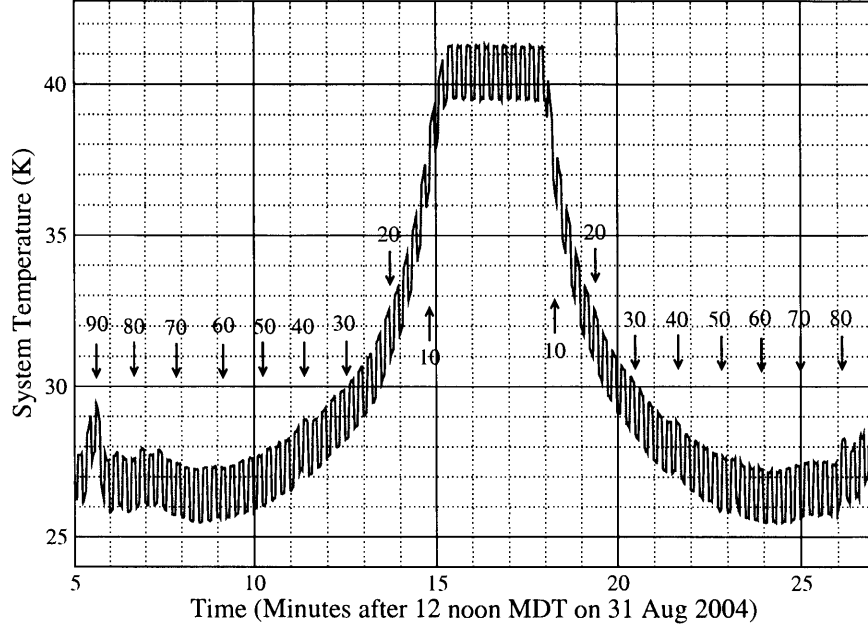


Figure 3: A tip scan for the EVLA test antenna at 1425 MHz. For this observation, the switched noise diode was left on. The observation was taken by a continuous motion at constant speed. The perturbation visible at $E = 90$ is due to the antenna beam or sidelobe passing through a background source. The oscillating system temperature is due to the noise diode switching at .067 Hz.

atmospheric contribution, $T_{atm} = 1.0 \sec(z)$ Kelvin (Bryan Butler, priv. comm.), then subtracting an offset equal to the remaining value at 60 degrees elevation. This offset is primarily due to the receiver temperature, but includes minor contributions from the 2.8K CMB, galactic emission, and the spillover at the fiducial elevation of 60 degrees. Excellent general agreement is seen in the residuals amongst the three lower frequencies, with the greatest spillover noted at the lowest frequency of 1325 MHz. The curve at 1925 MHz is less reliable, but the ‘bump’ near 30 degrees elevation is believed to be real.

A comparison of VLA and EVLA antenna performance is shown in Fig. 5. The spectacular improvement in low-elevation performance provided by the new feed design is quite evident.

The over-the-top observations showed no evidence of asymmetric spillover.

4.3 Cold Sky System Temperature

The measurements of the cold sky system temperature were taken from the minimum value of system temperature determined from the sky dips discussed in the preceding section – typically at an elevation of about 60 degrees. These results are listed in Table 1. Note that the system temperature at 1975 MHz is very high – this is a result of using the existing low-gain VLA receiver for these tests. With the new wide band receiver, we expect the cold sky temperature at this frequency to match that measured for the others.

In the table, we have attempted to separate the contributions from the receiver, atmosphere, galaxy, cosmic microwave background, and spillover. The listed receiver temperature is that measured on the bench. The ‘sky’ component comprises the atmospheric (1.0K) and CMB contributions (3.8K) and an estimated galactic component of $1.7\nu^{-2.75}$ K. There is larger error for the derived quantities at 1975 MHz, as described in the preceding section.

These values are to be compared to the 1425 MHz observations taken with VLA antennas 24

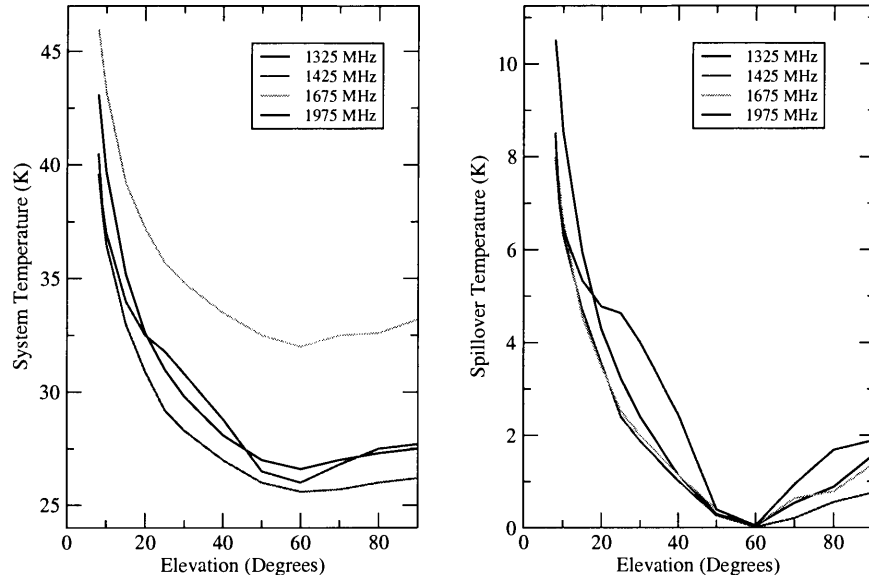


Figure 4: The dependence of system temperature on elevation for the EVLA test antenna. The left panel shows the total system temperature for the three lower frequencies, and an adjusted system temperature for 1975 MHz. The right panel shows the variation in the spillover contribution, after an offset equal to the value at 60 degrees elevation, and the expected atmospheric contribution has been subtracted. See the text for details.

System Temperature for El.= 60				
Frequency	T_{sys}	T_r	T_{sky}	T_{spill}
1325	26.7	12.2	4.6	9.9
1425	25.5	16.2	4.4	4.9
1675	32	17.2	4.2	10.6
1975	115	102	4.1	8.9

Table 1: The minimum cold-sky system temperature, and its separation into ‘sky’ emission (including atmosphere, CMB and galactic), receiver contributions, and spillover. The values for 1975 MHz are less accurate than the others. The receiver temperatures shown are from lab measurements.

and 28, for which the minimum system temperature was measured to be 31K. These two antennas were selected as comparisons as they have the same cooled hybrid polarizer as the EVLA antenna. The standard VLA polarizer is a dielectric wedge, for which the expected contribution to the system temperature is about 4K (Paul Lilie, priv. comm.). Thus, the EVLA system temperature, at high elevation, is expected to be 4 to 8K less than that of the old VLA antennas.

4.4 Antenna Efficiency, and System Equivalent Flux Density

The antenna efficiency is defined as the ratio between the actual power received by an antenna to that which traverses through an aperture of equal cross-section. In terms of the physical cross-section area, A_p , and the effective area A_e , we have

$$\epsilon = \frac{A_e}{A_p} \quad (12)$$

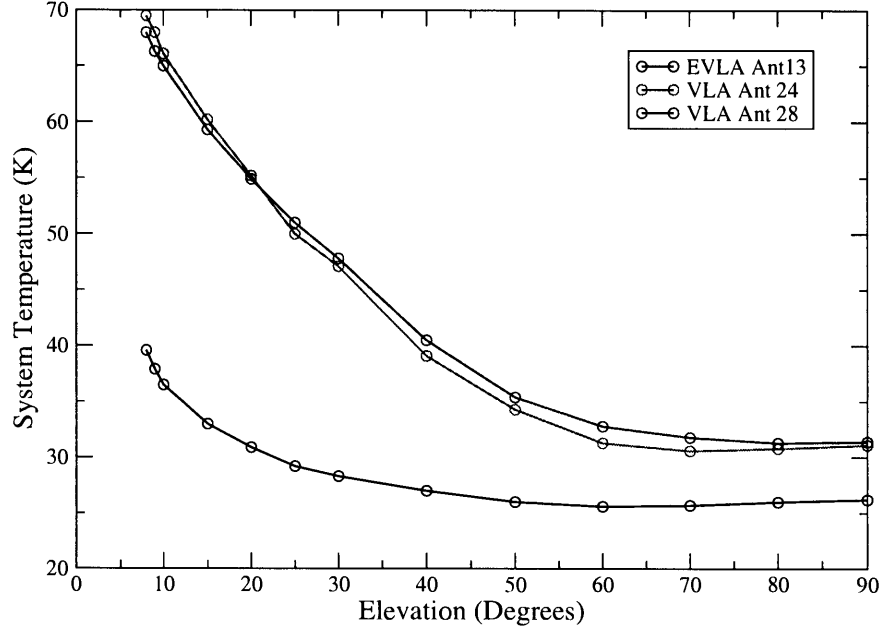


Figure 5: The variation of system temperature with elevation for the EVLA test antenna (13), and two VLA antennas (24 and 28) at 1425 MHz. These two VLA antennas were chosen for the measurement as they have the same cooled hybrid polarizer at the EVLA test antenna. Other VLA antennas retain the old dielectric polarizer, which adds about 4K to the system temperature.

Observation of a point object of known spectral flux density S_0 will result in an increase in antenna temperature by an amount

$$T_a = \frac{S_0 A_e}{2k} \quad (13)$$

where k is Boltzmann's constant.

With the antenna temperature in Kelvin, and the source flux density in Jy, the efficiency of a 25-meter antenna can be expressed as

$$\epsilon = 5.62 \frac{T_a}{S_{Jy}} \quad (14)$$

The efficiencies were determined by on-off observations of the well known calibrator Cygnus A. With an angular size of two arcminutes, no correction for angular size is needed. Because Cygnus A is located on the edge of the galactic plane, scans through the source were made to permit an accurate correction for the offset due to the galactic emission. The data, and results, are shown in Table 2.

EVLA Antenna L-Band Efficiency			
Frequency MHz	S Jy	T_a K	ϵ
1325	1680	135	0.45
1425	1558	121	0.43
1675	1315	102	0.44
1975	1101	105	0.54

Table 2: The EVLA L-band antenna efficiency, for various frequencies.

Observations of Cygnus A were also made with VLA antennas 24 and 28 at 1425 MHz. For both, the observed antenna temperature was 138K, giving an efficiency of 0.50.

Although the new feed has somewhat poorer efficiency, its overall performance is better, due to its lower system temperature. The appropriate performance metric is not the efficiency or system temperature, but rather their ratio. This is easily seen by noting that the point-source rms sensitivity of an interferometer can be written

$$\sigma_S = \frac{2kT_{sys}}{\epsilon A_p} \frac{1}{\sqrt{\delta\nu\delta t}} \frac{1}{\sqrt{N(N-1)}} = \frac{SEFD}{\sqrt{\delta\nu\delta t}\sqrt{N(N-1)}} \quad (15)$$

where the System Equivalent Flux Density, (*SEFD*), an important parameter of system performance, is defined as:

$$SEFD = \frac{2kT_{sys}}{\epsilon A_p} = \frac{T_{sys}S_0}{T_a}, \quad (16)$$

and the other terms account for the bandwidth-time product and the array collecting area. The *SEFD* is equal to the flux density of an object sufficient to double the system temperature.

The second form for *SEFD* shows how this parameter is determined from the observed antenna temperature from a source of known flux density and the antenna system temperature. In this latter form, the units of *SEFD* are Jy. The *SEFD* is simply the inverse of the ‘G/T’ parameter used by some antenna system designers.

At 1425 MHz, the *SEFD* for the VLA systems (with the new cooled hybrid polarizer) is found to be 350 Jy. For the new EVLA feed, we find *SEFD* = 335, slightly better than the VLA system. This difference is probably not significant, as the variation in receiver temperature between antennas is sufficient to explain this difference.

The observed FWHP for the EVLA test antenna was 20.6 arcminutes at 1975 MHz, and 29.35 arcminutes at 1425 MHz.

4.5 Antenna Beam and Sidelobes

The final measures made were of the antenna primary beamshape and the inner sidelobes. Ideally, we would have liked to have used the holographic raster scanning modes for this. However, the software to drive the EVLA antenna in this grid pattern is not yet available, so we utilized simple cross-cuts at various azimuths.

The results for the EVLA at 1425 MHz are shown in Figs. 6, and for the VLA in Fig. 7. A comparison of the two along the four principal azimuths is shown in 8.

At the top end of the band, the observations show very similar results, as shown in Fig 9.

5 Discussion

The large reduction in system temperature at lower elevations due to the removal of the lens will provide a significant improvement in the EVLA’s sensitivity over that of the VLA. To demonstrate this, we have generated an ‘equivalent *SEFD*’ for two observing scenarios at various declinations: A meridian snapshot, and a long-duration integration, where the integration was begun and ended at an elevation of ten degrees. The results are shown in Figure 10.

The ‘snapshot’ *SEFD*s (black lines) reflect the degradation of performance with elevation due to illumination spillover and scattering of ground radiation into the feeds. The performance is similar between the EVLA and VLA for high elevation observations (roughly, declinations between 0 and 60), and is notably better for the EVLA at more extreme declinations. The ‘integrated’ *SEFD*s (red lines) clearly show the greatly improved performance of the EVLA’s feed over that of the VLA. It

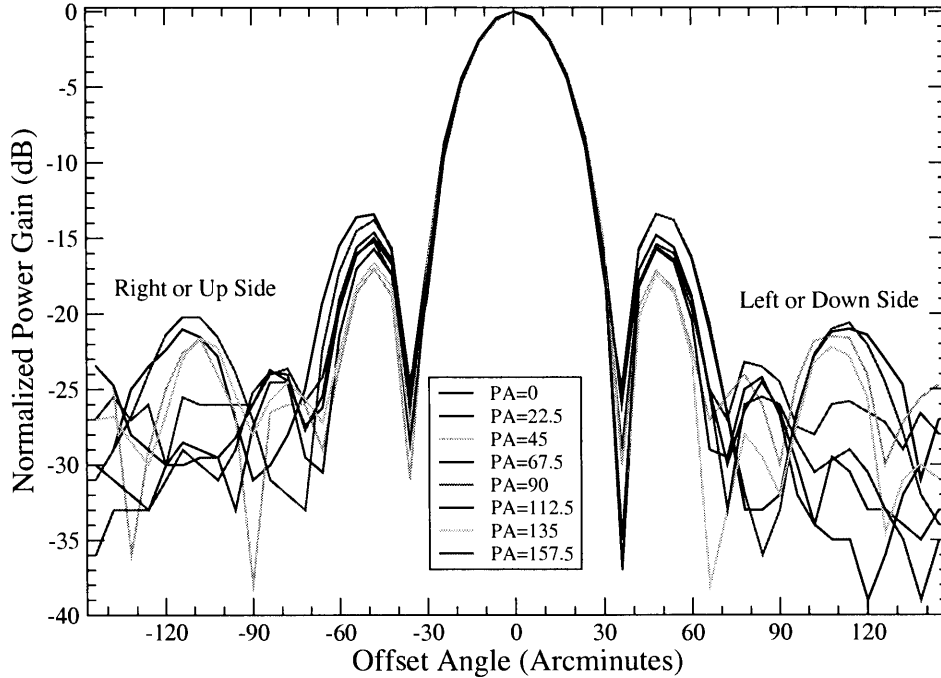


Figure 6: Eight cuts through the EVLA Antenna 13 at 1425 MHz. Zero azimuth is defined as 'up-down'. The sidelobe levels are higher in the horizontal and vertical cuts because of the quadrupod legs.

must be noted that these 'integrated SEFD' values were formed from unweighted averages over the integration periods, and hence will be biased upwards. A proper estimate must take into account the weighting actually utilized in the imaging process. We do not believe this more correct analysis would significantly change the conclusions.

6 Acknowledgement

This wide-band feed was designed by S. Srikanth. A detailed comparison of the predicted performance of the design to the characteristics described in this report will be made by Sri in a later memo.

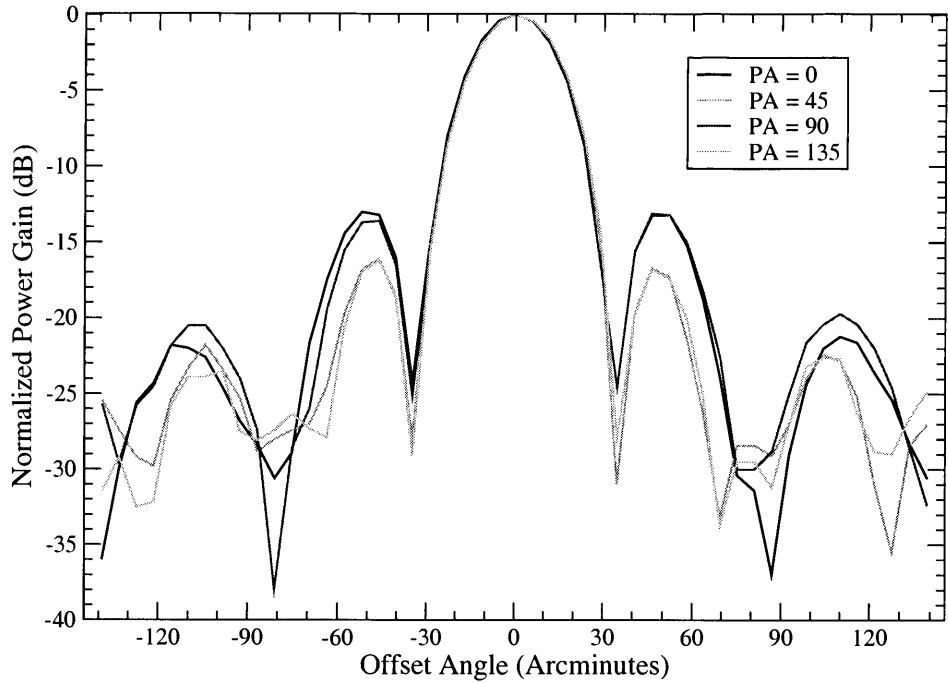


Figure 7: Four radial cuts through the VLA's power pattern at 1425 MHz. The patterns seen are very similar to those on the EVLA.

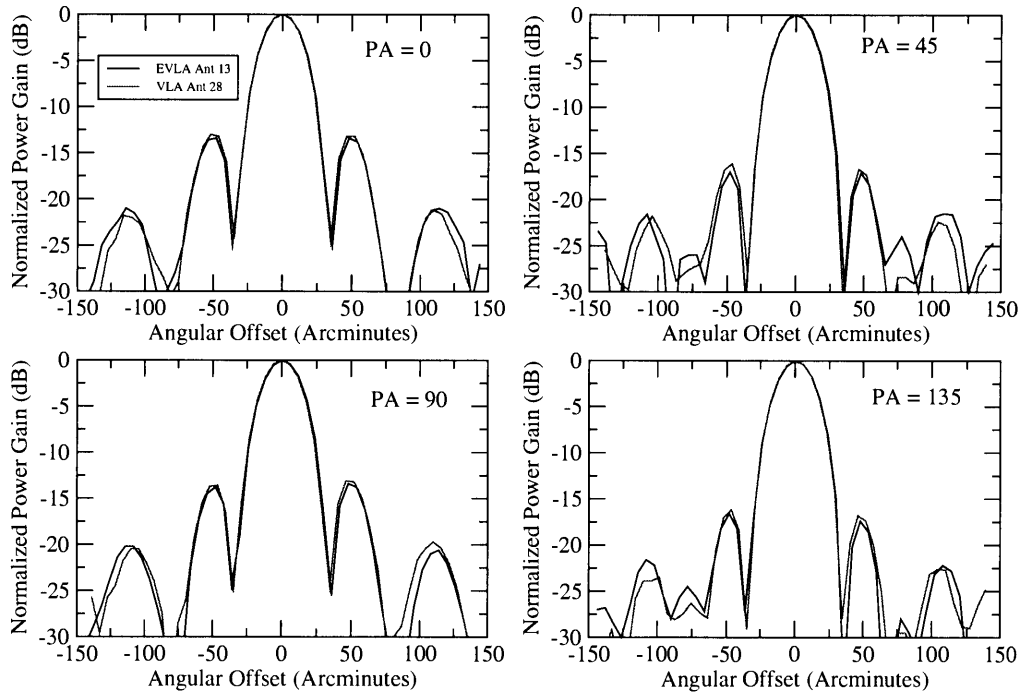


Figure 8: Four cuts through the EVLA and VLA beams superposed to permit direct comparison. The main beam and inner sidelobes are very similar. The EVLA's first sidelobe is marginally lower, indicating a slightly softer taper.

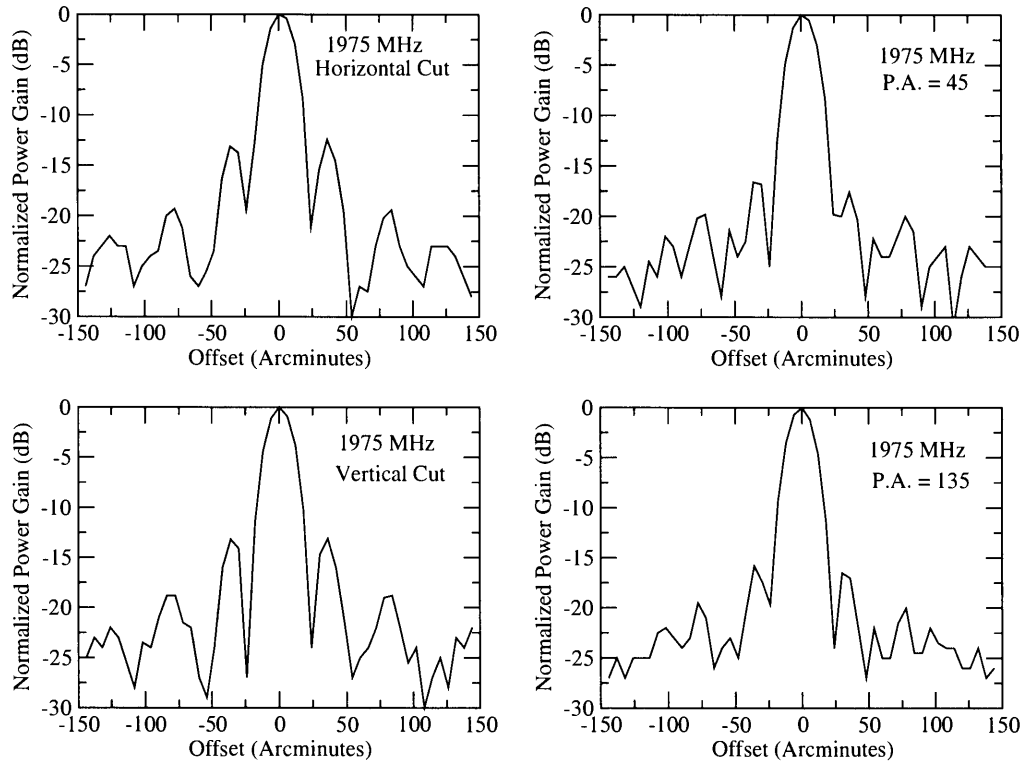


Figure 9: Four cuts through the EVLA test antenna at 1975 MHz. The sensitivity of these observations is lower, and values below -25 dB are not reliable.

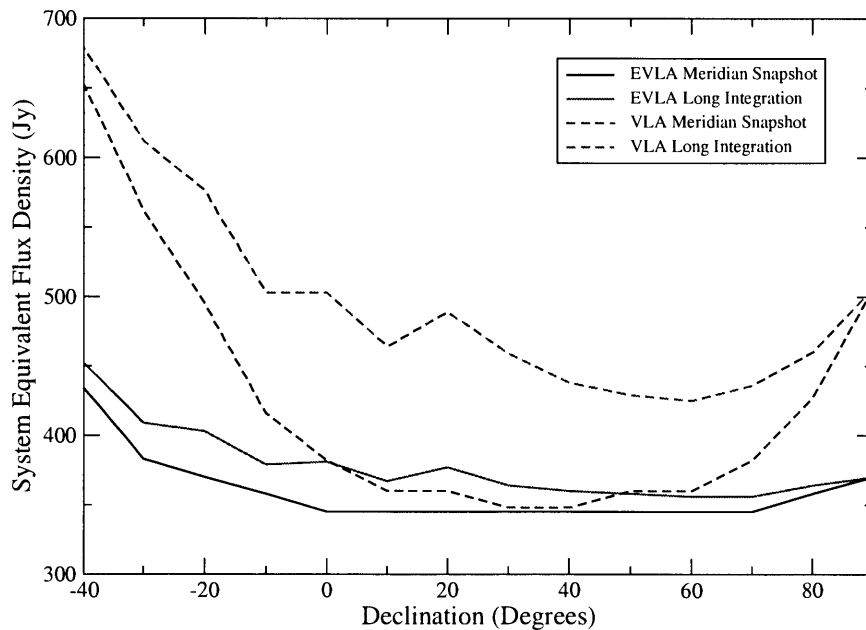


Figure 10: The averaged values of SEFD for the VLA and EVLA at 1425 MHz, as a function of declination and type of observation. The black lines show the SEFD for a meridian snapshot, the red lines show the average SEFD for a long integration. The dashed lines show the current VLA L-band performance, the solid lines show the expected EVLA performance.